
A fully 3D multi-path convolutional neural network with feature fusion and feature weighting for automatic lesion identification in brain MRI images

Yunzhe Xue

Department of Computer Science
New Jersey Institute of Technology
Newark, NJ, USA
yx277@njit.edu

Meiyan Xie

Department of Computer Science
New Jersey Institute of Technology
Newark, NJ, USA
mx42@njit.edu

Fadi G. Farhat

Department of Computer Science
New Jersey Institute of Technology
Newark, NJ, USA
fgf4@njit.edu

Olga Boukrina

Stroke Rehabilitation Research
Kessler Foundation
West Orange, NJ, USA
oboukrina@kesslerfoundation.org

A. M. Barrett

Stroke Rehabilitation Research
Kessler Foundation
West Orange, NJ, USA
abarrett@kesslerfoundation.org

Jeffrey R. Binder

Department of Neurology
Medical College of Wisconsin
Milwaukee, WI, USA
jbinder@mcw.edu

Usman W. Roshan

Department of Computer Science
New Jersey Institute of Technology
Newark, NJ, USA
usman@njit.edu

William W. Graves

Department of Psychology
Rutgers University - Newark
Newark, NJ, USA
william.graves@rutgers.edu

Abstract

Brain MRI images consist of multiple 2D images stacked at consecutive spatial intervals to form a 3D structure. Thus it seems natural to use a convolutional neural network with 3D convolutional kernels that would automatically also account for spatial dependence between the slices. However, 3D models remain a challenge in practice due to overfitting caused by insufficient training data. For example in a 2D model we typically have 150-300 slices per patient per plane of orientation whereas in a 3D setting this gets reduced to just one point. Here we propose a fully 3D multi-path convolutional network with custom designed components to better utilize features from multiple modalities. In particular our multi-path model has independent encoders for different modalities containing residual convolutional blocks, weighted multi-path feature fusion from different modalities, and weighted fusion modules to combine encoder and decoder features. We provide intuitive reasoning for different components along with empirical evidence to show that they work. Compared to existing 3D CNNs like DeepMedic, 3D U-Net, and AnatomyNet, our networks achieves the highest statistically significant cross-validation accuracy of 60.5% on the large ATLAS benchmark of 220 patients. We also test our model on multi-modal images from the Kessler Foundation and

Medical College Wisconsin and achieve a statistically significant cross-validation accuracy of 65%, significantly outperforming the multi-modal 3D U-Net and DeepMedic. Overall our model offers a principled, extensible multi-path approach that outperforms multi-channel alternatives and achieves high Dice accuracies on existing benchmarks.

1 Introduction

Lesion identification in brain MRI images is of considerable interest in neuroscience research and clinical work. In both settings neuroscientists produce a mapping of the lesion which is then used for downstream analysis. Lesion mappings can take between 4.8 and 9.6 hours [1] and agree 67-73% between different raters [2, 3]. In order to produce fast and accurate mappings automatically several machine and deep learning methods have been introduced.

The UNet [4] is one of the first end-to-end networks designed for medical image segmentation. Their U-shaped structure of downsampling encoders followed by upsampling decoders and connections between encoders and decoders is widely used in deep learning solutions for lesion detection in brain MRI images. Inspired by the success of novel convolutional blocks in ResNet [5] and DenseNet [6] new 2D segmentation models based on them have been introduced. For example residual blocks have been used for aerial road identification [7] and dense networks for lesion segmentation [8]. However, these are 2D convolutional models whereas the inputs are 3D images.

One major drawback of 2D methods is that they consider one slice of the 3D brain MRI image at a time whereas the slices are spatially connected in the 3D volume. Previously convolutional LSTMs [9] have been used to address the spatial dependency between slices. A more comprehensive and simpler approach is to use 3D convolutional kernels. However, training a 3D convolutional kernel is not easy: it has more parameters than a 2D kernel, is prone to overfitting, and requires more data.

One solution is to turn the input 3D image into smaller 3D cubes and then train on the cubes like DeepMedic [10]. This increases the training dataset size but performs poorly on small lesions as we show later. Smaller cube inputs provide less information to the network and thus we expect it to miss hard lesions. Other 3D convolutional networks such as AnatomyNet [11] use squeeze-and-excitation [12] to perform feature weighting.

Since brain MRI images typically come in different modalities several multi-modal ones have been proposed. These include DeepMedic [10], 3D U-Nets [13], and Dense U-Nets [8] with different feature fusion methods for different modalities. A simple way to combine multiple modalities is to stack them as multiple channels. This may not be the best approach because images from different modalities may have different pixel distributions and different range of pixel values unlike multiple channels in natural images such as RGB channels. Thus we take a multi-path approach where each modality has its own encoder.

Our contribution here is a fully 3D convolutional network that contains only 3D convolutional kernels, 3D feature fusion modules, and feature weighting methods. We use separate encoders for each modality which we then fuse in a custom designed feature fusion module. The fused features are then added to outputs from the upsampling blocks. We use squeeze-and-excitation to weigh channels for different modalities as well as a simple custom designed amplified weighting designed to fit small lesions that are hard to detect.

We start below with a description of our model and its components followed by an experimental performance study. In our study we compare our model to three other 3D convolutional networks on two brain MRI datasets. Overall our model obtains a statistically significant improvement over previous models thus demonstrating the effectiveness of our multi-path, fusions, and weighting techniques.

2 Methods

2.1 Fully 3D multi-path convolutional neural network

Our overall model structure is given in Figure 1. The U-shaped network with encoders, decoders, and connections between them is a widely used structure for segmentation problems [4]. In Table 1 we provide the input dimensions to each module and describe them in detail below.

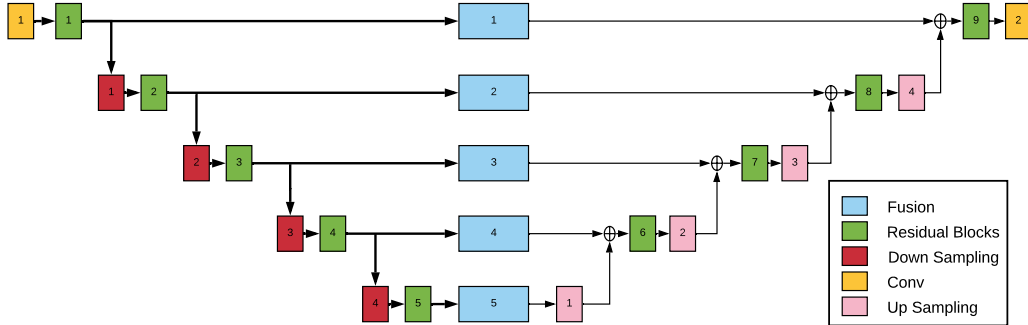


Figure 1: Overview of our 3D convolutional neural net system.

Table 1: Input dimensions to each component in our system, The first dimension is the number of channels followed by x, y, z dimensions of the input image. We denote by k the number of different modalities (one independent path per modality).

Input convolution (Conv 1)	16 single channel convolutional kernels in the first block per path, input shape is $k, 160, 192, 160$
Residual block 1, Fusion 1, Downsampling 1	$16k, 160, 192, 160$
Residual block 2, Fusion 2, Downsampling 2	$32k, 80, 96, 80$
Residual block 3, Fusion 3, Downsampling 3	$64k, 40, 48, 40$
Residual block 4, Fusion 4, Downsampling 4	$128k, 20, 24, 20$
Residual block 5, Fusion 5, Downsampling 5	$256k, 10, 12, 10$
Upsampling 1	$256, 10, 12, 10$
Residual block 6, Upsampling 2	$128, 20, 24, 20$
Residual block 7, Upsampling 3	$64, 40, 48, 40$
Residual block 8, Upsampling 4	$32, 80, 96, 80$
Residual block 9, output convolution (Conv 2)	$16, 160, 192, 160$

Residual convolutional blocks Our encoder has two convolutional layers and a residual connection to prevent gradient problems as shown in Figure 2(a). Where to put the residual connection after batch normalization in the convolutional block, for example after or before the ReLU activation layer, has been explored previously [14]. We take the most accurate *full pre-activation* option of adding the residual connection after the second convolutional filter. Each convolutional kernel is 3D of dimensions $3 \times 3 \times 3$, stride 1, and has the same number of output channels as the input. Since our batch sizes are small we use instance normalization [15], this also serves to reduce the influence of batch stochastic noise. We have a separate encoder for each image modality thus giving rise to a multi-path model where each path is independent.

Downsampling Instead of just pooling to downsample we take a dual-path approach. In addition to standard average pooling we use a convolutional layer to bring a non-linear component to filter out noise and acquire better high level semantic information. In Figure 2(b) we show a toy example 3D input to the downsampling with four channels. The four channels correspond to the output of the previous residual block. The actual dimensions are given in Table 1. We have a separate downsampler for each modality. Our pooling here is $3D 2 \times 2 \times 2$ with stride 2 and convolutions are also $3D 3 \times 3 \times 3$ with stride 2. We concatenate the outputs to preserve the channel order as shown in Figure 2(b). Thus the number of channels double after the downsampling block.

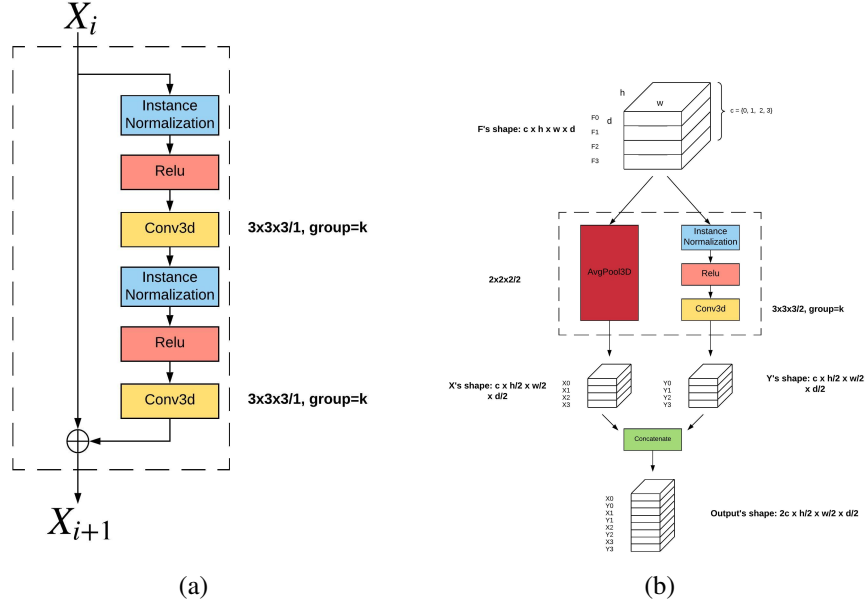


Figure 2: In (a) we see our residual convolutional block. We have a separate block for each modality in the input. In (b) we see our downsampling block that also has a convolutional component.

Feature fusion We combine features from multiple encoders in a fusion module before connecting them to upsampling components. As shown in Figure 3(b) our fusion module is a convolutional block except that the 3D kernel is $1 \times 1 \times 1$ with stride 1 and has $\frac{c}{k}$ channels. Here the inputs are combined multi-channel 3D images from different modalities all stacked into c channels. The output is one image with the same number of channels as per modality in the input.

We also investigate a more sophisticated fusion module that has a squeeze and excite block [12] (see Figure 3(a)). The purpose of this block is to automatically learn weights for different modalities by compressing features (with global average pooling and a 3D kernel) and then restoring to original channels with a 3D kernel.

Upsampling Our upsampling is a straightforward 3D transposed convolution with stride 2 to double the image dimensions. In Figure 3(c) we see the upsampling block in full. We see that the upsampling block has output channels equal to half the number of input channels, thus cutting the number of channels by two as we proceed upstream.

Loss function The output from the last convolutional layer has two channels each of dimensions $160 \times 192 \times 160$. The target lesion has the same dimensions but just one channel. The first channel in our output predicts the lesion and the second one predicts the complement of it. We convert the outputs of each channel into probabilities with softmax [16] and combined them into a modified Dice loss function [17, 18]. For a single channel output the Dice loss is defined to be $1 - D$ where $D(p) = \frac{2 \sum_i p_i r_i}{\sum_i p_i^2 + \sum_i r_i^2}$, p_i are the predicted softmax outputs of the channel, and r_i is 1 if the voxel has a lesion and 0 otherwise. If we are predicting the complement of the lesion then the values of r_i are flipped from 0 to 1 and 1 to 0. With our two channel output p and q our loss becomes $2 - (D(p) + D(q))$ where the latter $D(q)$ is for the complement. Thus our loss ranges from 0 to 2.

2.2 Model implementation

Our system was implemented using Pytorch [19], the source code for which is available on our GitHub site available upon acceptance. Our model's initial learning rate is 0.01. We have a custom adaptive method that decreases the rate by 5% if the current epoch's training loss is larger than that of previous epoch. We run our model for a total of 100 epochs for a given input training set. We use stochastic gradient descent (SGD) as the optimizer with nesterov. Our momentum parameter

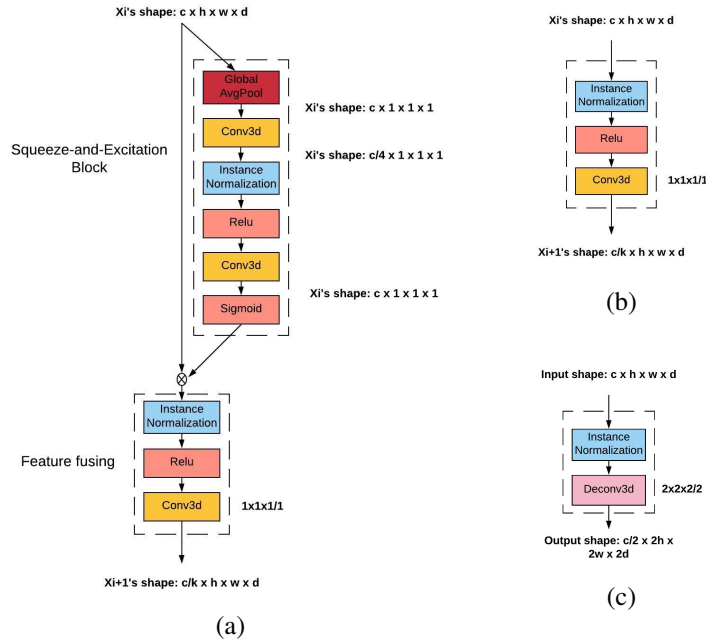


Figure 3: In (b) we have a simple fusion block that uses a $1 \times 1 \times 1$ 3D kernel with stride 1 and $\frac{c}{k}$ channels for merging the combined multi-modal input of c channels. In (a) we see the squeeze and excite module to give weights to different channel modalities. In (c) is our basic upsampling module.

is 0.9 with no weight decay. Our batch size is 4 trained on two GPUs where each GPU does 2 samples at a time. Our convolutional layer weights are initialized with ResNet’s weight initialization method [5].

2.3 Variants of our model

We study different designs of our model and demonstrate their accuracy on test data.

Single path Here we have a single encoder combined for all modalities. In this version different modalities are stacked as multiple channels. With this variant we can see the effect of a multi-channel vs. multi-path approach for different input modalities.

No fusion This applies only to ATLAS data where we have single modality T1 images. Since the images have just one modality there are no features to fuse. Thus we replace the fusion module with identity mapping as in the original 3D UNet.

Basic This is our basic multi-path model with the basic fusion component shown in Figure 3(b).

Squeeze-and-excitation in fusion (SE) Here we consider the fusion block with the squeeze-and-excitation component [12] in fusion to weigh channels across different modalities (Figure 3(a)). This is a kind of attention mechanism [20] focusing on channels. The idea is to use pooling to compress features to a point followed by fully connected layers and non-linear activation (sort of a mini encoder decoder setup). The sigmoid layer outputs a number between 0 and 1 that is used to weight the channel.

SE and Amplified Weighting (SE+AW) During our experimental design we found that small lesions are particularly hard to map. In fact our ATLAS benchmark has about a quarter of images with lesion volumes below $1000mm^3$ and a third quarter below $10000mm^3$. More interestingly we found 25 samples in ATLAS which give a 0 Dice coefficient during training. We call these *hard* samples and found their gradient values in the residual block in the decoder to be much smaller compared to

that of other samples (about one thousand times). One explanation for this is the addition operation between features from the upsampler (Figure 3(c)) and the fusion module (Figure 3(a) and (b)). Upon closer examination we find the output from the fusion to have a much larger value than the upsampler before entering the residual block (30 to 100 times). As a possible fix we simply amplify the weights from the upsampler by a factor of 10. We call this Amplified Weighting (AW).

ReLUOnly Instead of amplifying the upsampler weights as above we consider an alternative approach to balance the magnitude of outputs from the fusion and upsampler modules. In our residual block we move the first normalization layer in Figure 2(a) to the end as the final layer just before addition. This is known as the ReLU-Only pre-activation [14]. With this modification the outputs from the residual blocks get normalized to between 0 and 1. These are then given as inputs to the fusion module and because they are normalized the outputs from the fusion module are not much larger than the upsampler outputs (about 10 to 30 times). In fact the squeeze-and-excitation module that assigns weights to different channels is partly responsible for the weight inflation. This variant includes the SE variant above.

Flip This variant is for the ATLAS dataset only. Since we have only T1 images we use the flipped version of the image as a second modality. As we show in our results this leads to a considerable improvement in the test accuracy.

2.4 Data, other methods, measure of accuracy and statistical significance

Imaging Data We obtained high-resolution (1 mm³) whole-brain MRI scans from 25 patients from the Kessler Foundation (KES), a neuro-rehabilitation facility in West Orange, New Jersey. We also obtained 20 high-resolution scans from the Medical College of Wisconsin (MCW). Data heterogeneity is important for widespread applicability of the model. To that end, we included data from a variety of time points: subacute (< 5 weeks post stroke) and chronic (> 3 months post stroke). The lesions visualized on the scans were hand-segmented by a trained human expert, as described for the KES scans in [21] and the MCW scans [22, 23]. To move these scans into standard Montreal Neurological Institute (MNI) reference space [24], we used the non-linear warping tool, 3dQwarp, from the AFNI software suite [25].

We also obtained 220 scans and stroke lesion masks from the public ATLAS database [3]. These lesions are also manually performed and we aligned them in the same way that we did KES and MCW images. However, while KES and MCW are multi-modal the ATLAS images are just T1.

Comparison of CNN Methods We compared our CNN to three state of the art recently published CNNs shown below. We train each of the models below in the same way that we train our model as described earlier in Subsection 2.2.

- DeepMedic [10]: This is a popular dual-path 3D convolutional neural network with a conditional random field to account for spatial order of slices. DeepMedic contains a path for low- and a separate path for high-resolution of images. Its success was demonstrated by winning the ISLES 2015 competition to identify brain injuries, tumors, and stroke lesions. The code for implementing DeepMedic is freely available on GitHub, <https://github.com/Kamnitsask/deepmedic>.
- AnatomyNet [11]: This is a convolutional neural network with residual connections [5] and squeeze-excitation blocks [12]. The code for AnatomyNet is freely available on GitHub at <https://github.com/wentaozhu/AnatomyNet-for-anatomical-segmentation>.
- 3D-UNet [4]: A 3D U-Net that obtained third place in the BRATS 2017 multimodal brain tumor segmentation challenge. Its PyTorch implementation is freely available on GitHub at <https://github.com/pykao/Modified-3D-UNet-Pytorch>.

Measure of accuracy: Dice coefficient The Dice coefficient is typically used to measure the accuracy of predicted lesions in MRI images [26]. The output of our system and that of other methods is a binary mask of the same dimensions as the input image, but with a 1 for each voxel calculated to contain a lesion, and a 0 otherwise. Starting with the human binary mask as ground truth, each predicted voxel is determined to be either a true positive (TP, also one in true mask), false positive (FP, predicted as one but zero in the true mask), or false negative (FN, predicted as zero but one in the true mask). The Dice coefficient is formally defined as $DICE = \frac{2TP}{2TP+FP+FN}$.

Measure of statistical significance: Wilcoxon rank sum test The Wilcoxon rank sum test [27] (also known as the Mann-Whitney U test) can be used to determine whether the difference between two sets of measurements is significant. More formally, it tests for the null hypothesis that a randomly selected point from a sample is equally likely to be lower or higher than a randomly selected one from a second sample. It is a non-parametric test for whether two sets of observations are likely to be from different distributions, without assuming a particular shape for those distributions.

3 Results

We have two main subsections here. First we compare variants of our approach and pick the best one to compare against other programs. We perform a five-fold cross-validation. On KES+MCW our splits are chosen randomly whereas in ATLAS we first rank the samples by their training accuracy in increasing order. We then group every five together and rotate the test sample by picking the first from each group of five, then the second and so forth. This gives us five sets of train and test samples. Our goal here is to include hard to train samples in the training set so as to better predict hard ones in the test. We apply all methods to the same set of splits in both datasets.

Each of our MRI images is aligned to standard space. We crop them into $160 \times 192 \times 160$ size based on the brain template. We normalized each 3D image by subtracting the mean and dividing by variance of the image’s pixel values.

3.1 Effect of Amplified Weighting (AW)

We first show how amplifying gradient weights from the upsampling block affects training accuracy on hard samples. Recall that we define hard samples as 25 identified ones with 0 Dice value in training. In other words they are impossible to fit by the model without amplified weighting. In Figure 4(a) we see that by upweighting (simply multiplying the outputs by 10) our model is able to train the hard samples. In Figure 4(b) we see that amplified weighting also helps in model training. With the weighting the loss of hard samples starts to decrease after some epochs whereas otherwise it remains at 1.

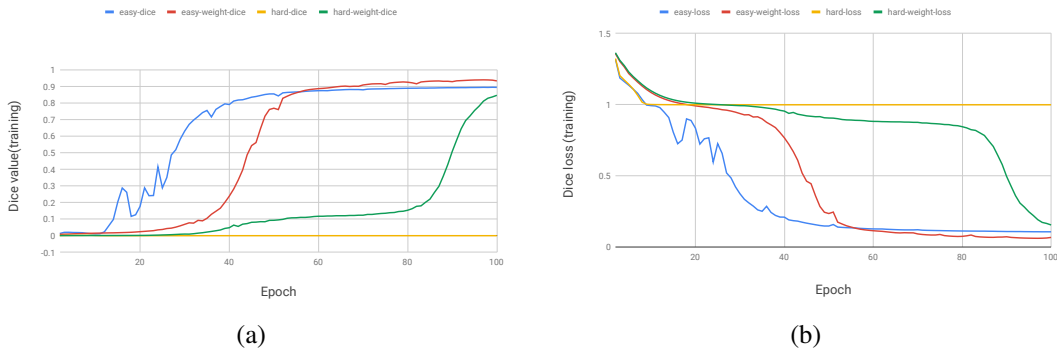


Figure 4: Training Dice value in (a) and Dice loss in (b) on hard vs rest (easy) samples with weighted and balanced connections to the residual blocks in the decoder. The two connections to be weighted are the outputs from the upsampler and fusion (the former of which turn out to be much smaller than fusion for hard samples).

3.2 Comparing variants of our model

In Figure 5 we compare the average Dice coefficients of test samples of each of our variants. On KES+MCW (Figure 5(a)) we see that our Basic variant (multi-path approach) has about a 2% improvement over the SinglePath variant that stacks different modalities as multiple channels. Thus treating each modality independently with their own encoders has a noticeable advantage. We see the same in ATLAS (Figure 5(b)) if we consider the flipped image as a second modality.

In fact in ATLAS we see that using the flipped image as another modality brings a considerable improvement over using just the single T1 images alone. The Flip variant in Figure 5(b) has 58.4%

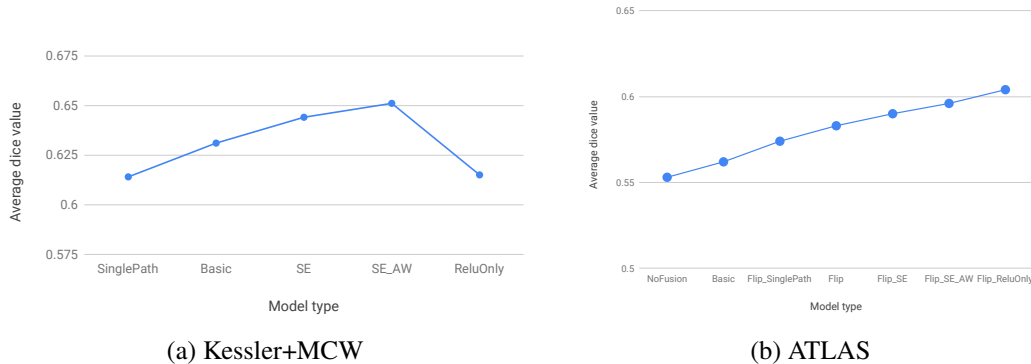


Figure 5: Average five-fold test Dice values of variants of our model on KES+MCW and ATLAS datasets.

Dice value whereas the Basic variant is at 56.3% (with the difference having a p-value of .086). Thus even a flipped image serving in a multi-path framework can bring an advantage. We conjecture that adding similar images as additional paths may further improve model generalizability and overall test accuracy.

Following the basic model we see that both squeeze and excite blocks and the amplified weighting improves overall test accuracy on both datasets. Thus upweighting features from the upsampler (as in our AW variant) help to improve not just training accuracy on hard samples but also the overall test accuracy. We see that the ReLUOnly variant works on ATLAS but performs much poorly on KES+MCW.

3.3 Comparison of our model to other 3D CNN models

In Figure 6 we compare our SE+AW (squeeze-and-excite in fusion and amplified weighting) model to three other 3D CNN models on KES+MCW. On ATLAS we show our ReLUOnly model although the SE+AW variant is only slightly behind in accuracy. On KES+MCW we do not have results for AnatomyNet since that is designed for single modality images. We show the Dice values for four different thresholds of lesion sizes starting from the smallest 25% to 100% that includes the entire dataset.

On KES+MCW we see that in the 25% smallest lesions our model has a 34.4% accuracy whereas the next best 3D U-Net is 29%. On ATLAS in the 25% smallest lesions our model has 41.4% accuracy while the next best AnatomyNet is 34.1%. Our weighting techniques (amplified weighting and ReLUOnly) thus give us a 5.4% and 7% improvement over the next best on KES+MCW and ATLAS respectively. In the case of ATLAS the improvement is statistically significant with a p-value of 0.004.

On all of KES+MCW (100% threshold) our model has a Dice value of 65.1% while the next best 3D U-Net reaches 60.8%. On all of ATLAS our model has Dice value 60.5% while the next best AnatomyNet reaches 56.1%. In both cases the differences are strongly statistically significant. On KES+MCW the difference has p-value 0.0016 and on ATLAS in the order of 10^{-6} . Thus we see that our model not only improves upon previous methods on small hard to detect lesions but overall as well.

4 Discussion

We see that flipping the T1 images gives a considerable boost to the accuracy of our model. In fact this is a novel approach to improve the accuracy of single modality images that has not been studied before. Taking this idea further we conjecture that adding similar images as another modality (as opposed to just flipping the input) may further improve model generalizability.

We conjecture our ReLUOnly variant’s poor performance on KES+MCW is likely due to its much smaller dataset size than ATLAS. We also gave T1 flipped images from ATLAS to the multi-modal

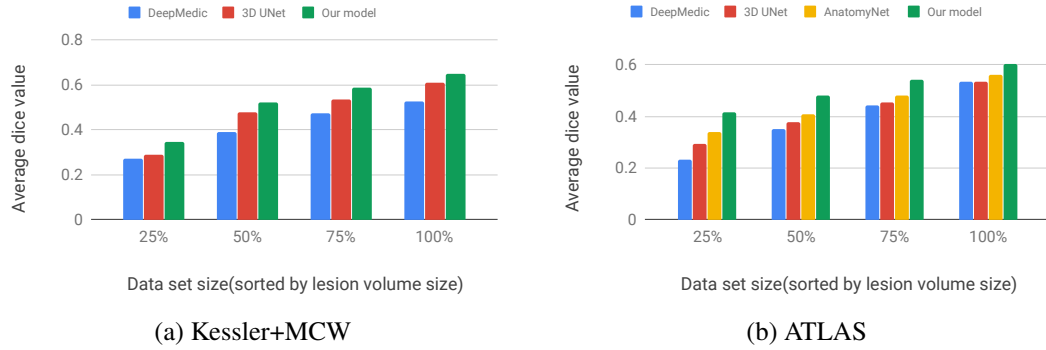


Figure 6: Average five-fold test Dice values of our SE+AW model compared to three other 3D CNNs on KES+MCW and ATLAS datasets.

3D U-Net and saw only a 1% rise in accuracy. This accuracy was still below that of AnatomyNet on ATLAS which we outperform by a statistically significant margin.

5 Conclusion

By building in the flexibility to weight contributions from different image modalities separately, and placing sufficient weight on up-sampled versions of the inputs that maintain information on smaller lesions, we have constructed a fully 3-dimensional model that outperforms comparable existing models. As a result, we have achieved a new level of accuracy in automated stroke brain lesion segmentation. This brings us a major step closer to removing a substantial barrier to progress in advancing studies of critical brain-behavior relationships.

References

- [1] Marko Wilke, Bianca de Haan, Hendrik Juenger, and Hans-Otto Karnath. Manual, semi-automated, and automated delineation of chronic brain lesions: A comparison of methods. *NeuroImage*, 56(4):2038 – 2046, 2011.
- [2] Julie A. Fiez, Hanna Damasio, and Thomas J. Grabowski. Lesion segmentation and manual warping to a reference brain: Intra- and interobserver reliability. *Human Brain Mapping*, 9(4):192–211, 2000.
- [3] Sook-Lei Liew, Julia M Anglin, Nick W Banks, Matt Sondag, Kaori L Ito, Hosung Kim, Jennifer Chan, Joyce Ito, Connie Jung, Nima Khoshab, et al. A large, open source dataset of stroke anatomical brain images and manual lesion segmentations. *Scientific data*, 5:180011, 2018.
- [4] Olaf Ronneberger, Philipp Fischer, and Thomas Brox. U-net: Convolutional networks for biomedical image segmentation. In *International Conference on Medical image computing and computer-assisted intervention*, pages 234–241. Springer, 2015.
- [5] Kaiming He, Xiangyu Zhang, Shaoqing Ren, and Jian Sun. Deep residual learning for image recognition. In *Proceedings of the IEEE conference on computer vision and pattern recognition*, pages 770–778, 2016.
- [6] Gao Huang, Zhuang Liu, Kilian Q Weinberger, and Laurens van der Maaten. Densely connected convolutional networks. In *Proceedings of the IEEE conference on computer vision and pattern recognition*, volume 1, page 3, 2017.
- [7] Zhengxin Zhang, Qingjie Liu, and Yunhong Wang. Road extraction by deep residual u-net. *IEEE Geoscience and Remote Sensing Letters*, 15(5):749–753, 2018.
- [8] Jose Dolz, Ismail Ben Ayed, and Christian Desrosiers. Dense multi-path u-net for ischemic stroke lesion segmentation in multiple image modalities. In *International MICCAI Brainlesion Workshop*, pages 271–282. Springer, 2018.
- [9] Kuan-Lun Tseng, Yen-Liang Lin, Winston Hsu, and Chung-Yang Huang. Joint sequence learning and cross-modality convolution for 3d biomedical segmentation. In *Computer Vision and Pattern Recognition (CVPR), 2017 IEEE Conference on*, pages 3739–3746. IEEE, 2017.
- [10] Konstantinos Kamnitsas, Christian Ledig, Virginia FJ Newcombe, Joanna P Simpson, Andrew D Kane, David K Menon, Daniel Rueckert, and Ben Glocker. Efficient multi-scale 3d cnn with fully connected crf for accurate brain lesion segmentation. *Medical image analysis*, 36:61–78, 2017.
- [11] Wentao Zhu, Yufang Huang, Liang Zeng, Xuming Chen, Yong Liu, Zhen Qian, Nan Du, Wei Fan, and Xiaohui Xie. Anatomynet: Deep learning for fast and fully automated whole-volume segmentation of head and neck anatomy. *Medical physics*, 46(2):576–589, 2019.
- [12] Jie Hu, Li Shen, and Gang Sun. Squeeze-and-excitation networks. In *Proceedings of the IEEE conference on computer vision and pattern recognition*, pages 7132–7141, 2018.
- [13] Fabian Isensee, Philipp Kickingereder, Wolfgang Wick, Martin Bendszus, and Klaus H Maier-Hein. Brain tumor segmentation and radiomics survival prediction: contribution to the brats 2017 challenge. In *International MICCAI Brainlesion Workshop*, pages 287–297. Springer, 2017.
- [14] Kaiming He, Xiangyu Zhang, Shaoqing Ren, and Jian Sun. Identity mappings in deep residual networks. In *European conference on computer vision*, pages 630–645. Springer, 2016.
- [15] Yuxin Wu and Kaiming He. Group normalization. In *Proceedings of the European Conference on Computer Vision (ECCV)*, pages 3–19, 2018.
- [16] Ethem Alpaydin. *Machine Learning*. MIT Press, 2004.
- [17] Fausto Milletari, Nassir Navab, and Seyed-Ahmad Ahmadi. V-net: Fully convolutional neural networks for volumetric medical image segmentation. In *2016 Fourth International Conference on 3D Vision (3DV)*, pages 565–571. IEEE, 2016.
- [18] Ken CL Wong, Mehdi Moradi, Hui Tang, and Tanveer Syeda-Mahmood. 3d segmentation with exponential logarithmic loss for highly unbalanced object sizes. In *International Conference on Medical Image Computing and Computer-Assisted Intervention*, pages 612–619. Springer, 2018.
- [19] Adam Paszke, Sam Gross, Soumith Chintala, Gregory Chanan, Edward Yang, Zachary DeVito, Zeming Lin, Alban Desmaison, Luca Antiga, and Adam Lerer. Automatic differentiation in pytorch. In *NIPS-W*, 2017.
- [20] Ashish Vaswani, Noam Shazeer, Niki Parmar, Jakob Uszkoreit, Llion Jones, Aidan N Gomez, Łukasz Kaiser, and Illia Polosukhin. Attention is all you need. In *Advances in neural information processing systems*, pages 5998–6008, 2017.
- [21] Olga Boukrina, AM Barrett, Edward J Alexander, Bing Yao, and William W Graves. Neurally dissociable cognitive components of reading deficits in subacute stroke. *Frontiers in human neuroscience*, 9:298, 2015.

- [22] Sara B Pillay, Benjamin C Stengel, Colin Humphries, Diane S Book, and Jeffrey R Binder. Cerebral localization of impaired phonological retrieval during rhyme judgment. *Annals of neurology*, 76(5):738–746, 2014.
- [23] Jeffrey R Binder, Sara B Pillay, Colin J Humphries, William L Gross, William W Graves, and Diane S Book. Surface errors without semantic impairment in acquired dyslexia: a voxel-based lesion–symptom mapping study. *Brain*, 139(5):1517–1526, 2016.
- [24] Vladimir Fonov, Alan C Evans, Kelly Botteron, C Robert Almli, Robert C McKinstry, D Louis Collins, Brain Development Cooperative Group, et al. Unbiased average age-appropriate atlases for pediatric studies. *Neuroimage*, 54(1):313–327, 2011.
- [25] Robert W Cox. Afni: software for analysis and visualization of functional magnetic resonance neuroimages. *Computers and Biomedical research*, 29(3):162–173, 1996.
- [26] Alex P Zijdenbos, Benoit M Dawant, Richard A Margolin, and Andrew C Palmer. Morphometric analysis of white matter lesions in mr images: method and validation. *IEEE transactions on medical imaging*, 13(4):716–724, 1994.
- [27] Frank Wilcoxon. Individual comparisons by ranking methods. *Biometrics bulletin*, 1(6):80–83, 1945.